# Periodic DFTB for Supported Clusters: Implementation and Application on Benzene Dimers Deposited on Graphene

Mathias Rapacioli, Nathalie Tarrat

MDPI

*Article*

# Periodic DFTB for supported clusters : Implementation and application to benzene dimers deposited on graphene

**Mathias Rapacioli [1,*] and Nathalie Tarrat [2,*]**

[1] Laboratoire de Chimie et Physique Quantiques LCPQ/FERMI, UMR5626, Université de Toulouse (UPS) and CNRS, 118 Route de Narbonne, F-31062 Toulouse, France
[2] CEMES, CNRS, Université de Toulouse, 29 Rue Jeanne Marvig, 31055, Toulouse, France
* Correspondence: mathias.rapacioli@irsamc.ups-tlse.fr (M. R.) ; nathalie.tarrat@cemes.fr (N. T.)

**Abstract:** The interest for properties of clusters deposited on surfaces has grown in the recent years. In this framework the Density Functional based Tight Binding (DFTB) method appears as a promising tool due to its ability to treat extended systems at the quantum level with a low computational cost. We report the implementation of periodic boundary conditions for DFTB within the deMonNano code with **k**-points formalism and corrections for intermolecular interactions. The quality of the DFTB calculations is evaluated by comparison with dispersion-corrected DFT calculations. Optimized lattice properties for a graphene sheet and graphite bulk are in agreement with reference data. The deposition of both benzene monomer and dimers on graphene are investigated and the observed trends are similar at the DFT and DFTB levels. Moreover, interaction energies are of similar orders of magnitude for these two levels of calculation. This study has evidenced the high stability of a structure made of two benzene molecules deposited close to each other on the graphene sheet. This work demonstrates the ability of the new implementation to investigate surface deposited molecular clusters properties.

**Keywords:** Periodic DFTB; Benzene dimers; Graphene

**Citation:** Rapacioli, M.; Tarrat, N. Periodic DFTB for supported clusters : Implementation and application to benzene aggregates deposited on graphene. *Journal Not Specified* **2022**, *1*, 0. https://doi.org/

Received:
Accepted:
Published:



## 0. Introduction

The modelling of functional extended surfaces has grown in past decades to investigate, for fundamental and engineering purposes, a large number of phenomena or applications such as e.g. deposition [1], growth and migration [2], 2D assembly [3], catalysis [4], electrocatalysis [5], photocatalysis [6], molecular electronics [7], depollution [8], sensing [9]... Many of these studies have focused on deposited clusters, i.e. finite aggregations of basis elements (atoms or molecules) adsorbed on surfaces. Indeed, the physico-chemical properties of a cluster are distinct from the ones of both the single entities and the infinite cluster (bulk) and strongly depend on the size and structure of the cluster [10]. Understanding and controlling the structuration of deposited clusters could thus allow a precise tuning of their properties.

The theoretical study of clusters deposited on extended surfaces is very challenging due to the size of the space of structural and electronic configurations to be explored and to the high level of computational methods that has to be implemented. Indeed, the a priori unknown nature of the interactions between the cluster building blocks and between the cluster and the surface (with potential charge transfers at the cluster-surface interface) prevents the use of empirical force fields in favor of methods in which the electronic structure is explicitly considered. The very high computational cost of *ab initio* and Density Functional Theory (DFT) methods prohibiting their use for the study of such systems, particularly when dealing with global optimisation or finite-temperature molecular dynamics, one strategy consists in implementing in a periodic formulation approximate quantum mechanical methods. Among them, DFTB is an approximated DFT schemes with a much lower computational cost enabled by the use of

parameterised integrals in a minimal valence basis set [11–14]. There have been several implementations of DFTB within periodic conditions in various codes [15–21], allowing to compute structural, mechanical and electronic properties. In the present work, we report a new implementation of the DFTB scheme for periodic systems within the deMonNano code [22] combined with corrections to describe long range intermolecular interactions.

The model system chosen for assessing the performance of this implementation consists in benzene dimers deposited on a graphene surface. This system is relevant in an astrophysical context as it can be seen as a simple model of Polycyclic Aromatic Hydrocarbons (PAH) clusters adsorbed on large carbonaceous grains or on very large PAHs. Indeed, despite PAHs are expected to be ubiquituous in the interstellar medium [23] and their clusters have been proposed to play a significant role in the interstellar physics and chemistry [24], the structural and energetic property changes induced by their deposition on a surface remain to a large extend unknown. The second motivation for selecting this benchmark system is that a reasonable description of the benzene dimers potential energy surface is challenging even with *ab initio* schemes [25], making it a system of choice to address the quality our approach. This is due to the fine equilibrium between Pauli repulsion, dispersion and coulomb interaction, which drives the competition between parallel and T-shaped structures. In the past, we have shown that the combination of DFTB with empirical dispersion and atomic charges corrections allowed for a proper description of such systems [26].

In this paper, the periodic formulation of DFTB which has been implemented in deMonNano is presented in section 1, with a special focus on the originality of the present scheme with respect to other periodic implementations i.e. its combination with the WMull charge correction approach. Computational details are given in section 2 and the applications to graphene, graphite and benzene monomer and dimers deposited on graphene are discussed in section 3. Finally a conclusion is given in section 4.

## 1. Methods

### *1.1. DFTB*

The Density Functional based Tight-Binding method (DFTB) can be derived from DFT from several approximations [11,13,14,16,27].

The first one relies on expression of molecular orbitals (MOs) $\phi_i(\mathbf{r})$ as linear combinations of atomic orbital (LCAO)-type basis sets using minimal valence bases $\chi_\mu$.

$$\phi_i(\mathbf{r}) = \sum_\mu c_{i\mu}\chi_\mu(\mathbf{r}) \tag{1}$$

A Taylor expansion of the DFT energy is done as a function of the electronic density, the real density $\rho$ of the system minimizing the Kohn-Sham energy being searched as a perturbation with respect to a reference density $\rho_0$ ($\rho = \rho_0 + \delta\rho$) :

$$\begin{aligned} E[\rho(r)] = E[\rho_0(\mathbf{r})] + \int \left.\frac{\delta E[\rho(\mathbf{r})]}{\delta\rho(\mathbf{r})}\right|_{\rho_0} \delta\rho(\mathbf{r}) + \frac{1}{2}\int\int \left.\frac{\delta^2 E[\rho(\mathbf{r})]}{\delta\rho(\mathbf{r})\delta\rho(\mathbf{r}')}\right|_{\rho_0} \delta\rho(\mathbf{r})\delta\rho(\mathbf{r}') + \\ \ldots + \frac{1}{p!}\int\int\ldots\int \left.\frac{\delta^p E[\rho(\mathbf{r})]}{\delta\rho(\mathbf{r})\delta\rho(\mathbf{r}')\ldots\delta\rho(\mathbf{r}^{(\mathbf{p})})}\right|_{\rho_0} \delta\rho(\mathbf{r})\delta\rho(\mathbf{r}')\ldots\delta\rho(\mathbf{r}^{(\mathbf{p})}) \end{aligned} \tag{2}$$

In the original version, also known as the non self-consistent DFTB (sometimes referred to as zeroth-order DFTB or simply DFTB [11,12]), only the zeroth and first order terms of the Taylor expansion are retained. In the DFTB2 scheme [27], also known as self-consistent charge (SCC) DFTB, and in the DFTB3 scheme [28], the second and third order terms are also taken into account, respectively.

At the DFTB0 level, the potential energy reads :

$$E^{DFTB0} = \sum_{\alpha<\beta} E_{rep}(\mathbf{r}_{\alpha\beta}) + \sum_{i\mu\nu} n_i c_{i\mu} c_{i\nu} H^0_{\mu\nu} \tag{3}$$

with $E_{rep}(\mathbf{r}_{\alpha\beta})$ a repulsive contribution between atoms $\alpha$ and $\beta$, $n_i$ the occupation of the orbital $i$ and $H^0_{\mu\nu}$ the matrix elements associated to the Kohn Sham operator at the reference density expressed in the atomic basis. Its matrix elements, as well as those of the atomic overlap matrix $S$, can be parameterized as only one- or two-body terms. This is allowed by the definition of the reference density as a superposition of atomic densities $\rho_0 = \rho^\alpha_0 + \rho^\beta_0 + \rho^\gamma_0 + ...$ and the reduction of integrals to one- or two-center terms :

- $H^0_{\mu,\nu\in\alpha}(\rho_0) \approx H^0_{\mu\nu}(\rho^\alpha_0) \approx \delta_{\mu\nu}\epsilon_{\mu\alpha}$; the atomic orbital energies of the isolated atom $\alpha$
- $H^0_{\mu\in\alpha,\nu\in\beta}(\rho_0) \approx H^0_{\mu\nu}(\rho^\alpha_0 + \rho^\beta_0)$ which only depends on the distance between the two corresponding atomic centers : $H^0_{\mu\in\alpha,\nu\in\beta}(\mathbf{r}_\alpha - \mathbf{r}_\beta)$

Focusing from now on the SCC-DFTB level[27], the previous energy expression becomes :

$$E^{SCC-DFTB} = E^{DFTB0} + \frac{1}{2}\sum_{\alpha\beta} \gamma_{\alpha\beta} q_\alpha q_\beta \tag{4}$$

The last term corresponds to the second-order contribution and depends on the electronic density fluctuation $\delta\rho$ represented by atomic charges $q_\alpha$. $\gamma_{\alpha\beta}$ is a matrix whose diagonal terms are equal to the atomic Hubbard parameters and off-diagonal terms contain the $1/R$ coulomb interaction between atomic charges and an exchange-correlation energy contribution:

$$\gamma_{\alpha\beta} = \int\int \left( \frac{1}{|\mathbf{r}-\mathbf{r}'|} + \left.\frac{\delta^2 E_{xc}}{\delta\rho(\mathbf{r})\delta\rho(\mathbf{r}')}\right|_{\rho_0} \right) F^\alpha_0(\mathbf{r}-\mathbf{r}_\alpha) F^\beta_0(\mathbf{r}'-\mathbf{r}_\beta) d\mathbf{r} d\mathbf{r}' \tag{5}$$

where $F^\alpha_0$ is the normalised spatial extension for the excess/default of electrons around atom $\alpha$ with respect to the neutral atom, assumed here to have no angular dependence.

Since the second-order term contains atomic charges, this introduces a term depending on the charges $H^1(q)$ into the TB operator.

$$(H^0 + H^1(q))C_i = \epsilon_i S C_i \tag{6}$$

with

$$H^1_{\mu\nu} = \frac{1}{2} S_{\mu\nu} \sum_\xi q_\xi (\gamma_{\alpha\xi} + \gamma_{\beta\xi})$$

where $\mu$ and $\nu$ belong to atoms $\alpha$ and $\beta$, respectively. As the charges depend on the MO coefficients $c_{i\mu}$, the new secular equation must be solved self-consistently with respect to atomic charges, at the origin of the method's name self-consistent-charge (SCC-)DFTB.

In the standard SCC-DFTB version [27], the atomic charges are computed from the density matrix $P$ and the atomic basis overlap $S$ matrix within the Mulliken approximation.

$$q_\alpha = \sum_{\mu\in\alpha}\sum_\nu P_{\mu\nu} S_{\mu\nu} \tag{7}$$

with

$$P_{\mu\nu} = \sum_{\mu\nu} n_i c_{i\mu} c_{i\nu}$$

In previous works, we have shown that atomic charges can be improved by taking into account the bond polarisation, adapting the Charge Model class IV scheme for DFTB [26,29]. This approach, which requires the calculation of Mayer's bond order, is computationally expensive and hardly transferable to a periodic implementation. To

circumvent this bottleneck, we have recently introduced a simpler scheme, named in the following WMull for Weighted Mulliken charges [30], to correct atomic charges with the following expression

$$q_\alpha = \sum_{\mu\in\alpha}\sum_{\nu} P_{\mu\nu}S_{\mu\nu}(1+t_{\alpha\beta}) \tag{8}$$

$t_{\alpha\beta} = -t_{\beta\alpha}$ is an empirical parameter accounting for a non-symmetric repartition of the electrons between different atomic types, the Mulliken symmetric repartition being recovered for $t_{\alpha\beta} = 0$. The second order contribution to the Kohn Sham operator matrix is modified as follows :

$$H^1_{\mu\nu} = \frac{1}{2}S_{\mu\nu}\sum_{\xi} q_\xi(\gamma_{\alpha\xi}(1+t_{\alpha\beta}) + \gamma_{\beta\xi}(1-t_{\alpha\beta})) \tag{9}$$

We have shown that this simple scheme provides similar results to those obtained with the Charge Model approach to model clusters of PAHs [31] and water [32].

### *1.2. DFTB for periodic systems*

The former implementation of periodic DFTB within deMonNano was restricted to the Γ-point approximation only [22]. In the present implementation, the electronic problem is searched self consistently after defining a set of **k**-points in the reciprocal space. A step of the self-consistent scheme consists in solving separately the secular equations for each **k**-point to obtain the molecular orbitals $\phi_i^{\mathbf{k}}$. Molecular orbitals obtained for all **k**-point are then used to build the total electronic density, the latter being used as an input for the next self-consistent step.

For a given **k**-point, the molecular orbitals $\phi_i^{\mathbf{k}}$ must full-fill the Bloch-Theorem, that is

$$\hat{T}_{\mathbf{R}}\phi_i^{\mathbf{k}} = e^{i\mathbf{kR}}\phi_i^{\mathbf{k}}(\mathbf{r}) \tag{10}$$

where $\hat{T}_{\mathbf{R}}$ is the operator associated to a translation of **R**, where **R** is a vector connecting two unit cells. This is achieved by expanding the MOs on an basis of Bloch functions built from the real space atomic orbitals.

$$\phi_i^{\mathbf{k}}(\mathbf{r}) = \sum_{\mathbf{k}} c_{i\mu}^{\mathbf{k}}\chi_\mu^{\mathbf{k}}(\mathbf{r})$$

with

$$\chi_\mu^{\mathbf{k}}(\mathbf{r}) = \frac{1}{\sqrt{N}}\sum_N e^{i\mathbf{kR_N}}\chi_\mu(\mathbf{r}-\mathbf{R_N}) \tag{11}$$

where the infinite sum relies on all the possible translation from the main unit cell to any of the other ones. The overlap and Kohn Sham operator matrices expressed in this basis can be written from their real-space equivalent making use of the following transformation :

$$H^{\mathbf{k}}_{\mu\nu} = \sum_N e^{i\mathbf{kR_N}}H_{\mu\nu}(\mathbf{r}_\alpha - \mathbf{r}_\beta - \mathbf{R}_N) = \sum_N e^{i\mathbf{kR_N}}(H^0_{\mu\nu}(\mathbf{r}_\alpha - \mathbf{r}_\beta - \mathbf{R}_N) + H^1_{\mu\nu}(\mathbf{r}_\alpha - \mathbf{r}_\beta - \mathbf{R}_N))$$

and

$$S^{\mathbf{k}}_{\mu\nu} = \sum_N e^{i\mathbf{kR_N}}S_{\mu\nu}(\mathbf{r}_\alpha - \mathbf{r}_\beta - \mathbf{R}_N) \tag{12}$$

where $\mu$ and $\nu$ belong to atoms $\alpha$ and $\beta$, respectively.

In the previous expressions, the matrix elements of $H^0$ and $S$ are easily obtained from the DFTB Slater Koster tables and rapidly vanish for large values of $\mathbf{R}_N$. The first

order contribution to $H_{\mu\nu}$ is also short range with respect to $(\mathbf{r}_\alpha - \mathbf{r}_\beta - \mathbf{R}_N)$ but contains an infinite long range coulomb sum :

$$H^{1,\mathbf{k}}_{\mu\nu}(\mathbf{r}_\alpha - \mathbf{r}_\beta - \mathbf{R}_N) = \frac{1}{2} S_{\mu\nu}(\mathbf{r}_\alpha - \mathbf{r}_\beta - \mathbf{R}_N) \sum_\xi \sum_N q_\xi (\gamma_{\alpha\xi}(\mathbf{r}_\alpha - \mathbf{r}_\xi - \mathbf{R}_N) + \gamma_{\beta\xi}(\mathbf{r}_\beta - \mathbf{r}_\xi - \mathbf{R}_N)) \tag{13}$$

In practice, this infinite sum is replaced by an Ewald summation. The secular equation is solved for each **k**-point :

$$H^{\mathbf{k}} C^{\mathbf{k}}_i = \epsilon^{\mathbf{k}}_i S^{\mathbf{k}} C^{\mathbf{k}}_i \tag{14}$$

The eigenvalues $\epsilon^{\mathbf{k}}_i$ resulting from all the **k**-point secular equations are then sorted in ascending order to drive the determination of $n^{\mathbf{k}}_i$, the orbital occupation number following either a canonical occupation or a Fermi distribution.

The density matrix can therefore be computed for each **k**-point

$$P_{\mu\nu}(\mathbf{k}) = \sum_i n^{\mathbf{k}}_i c^{\mathbf{k}*}_{i\mu} c^{\mathbf{k}}_{i\nu} \tag{15}$$

We follow the approach of reference [15], which consists in building the real space density matrix and computing atomic charges in the real space. The real space density matrix is obtained by summing over the **k**-points :

$$P_{\mu\nu}(\mathbf{R_N}) = \sum_{\mathbf{k}} P_{\mu\nu}(\mathbf{k}) e^{-i\mathbf{k}\mathbf{R_N}} \tag{16}$$

and Mulliken charges are then computed as follows :

$$q_\alpha = \sum_{R_N} P_{\mu\nu}(\mathbf{R_N}) S_{\mu\nu}(\mathbf{r}_\alpha - \mathbf{r}_\beta - \mathbf{R}_N) \tag{17}$$

and used as inputs for the next SCC cycle.

The simple WMull correction to Mulliken charges can be generalised to the periodic equations replacing equation 17 and 13 by

$$q_\alpha = \sum_{R_N} P_{\mu\nu}(\mathbf{R_N}) S_{\mu\nu}(\mathbf{r}_\alpha - \mathbf{r}_\beta - \mathbf{R}_N)(1 + t_{\alpha\beta}) \tag{18}$$

and

$$H^{1,\mathbf{k}}_{\mu\nu}(\mathbf{r}_\alpha - \mathbf{r}_\beta - \mathbf{R}_N) = \frac{1}{2} S_{\mu\nu}(\mathbf{r}_\alpha - \mathbf{r}_\beta - \mathbf{R}_N) \sum_\xi \sum_N \begin{array}{ll} q_\xi & (\gamma_{\alpha\xi}(\mathbf{r}_\alpha - \mathbf{r}_\xi - \mathbf{R}_N)(1 + t_{\alpha\beta}) \\ & + \quad \gamma_{\beta\xi}(\mathbf{r}_\beta - \mathbf{r}_\xi - \mathbf{R}_N)(1 - t_{\alpha\beta})) \end{array}$$

## 2. Computational details

### *2.1. DFTB calculations*

Different DFTB parameters are available in the literature (cf. website www.dftb.org), depending on the choices made during the parameterization procedure such as the DFT functional, the basis sets type (Gaussian, Lorentzian) used to generate the atomic orbitals, the confinement imposed on these orbitals, the reference data used to compute the repulsive contribution $E_{rep}$ and, for the second and third order DFTB, the values of the atomic Hubbard parameters and their derivatives. In this work, we are working with the BIO DFTB set of parameters [27] provided within the deMonNano code (equivalent to the mio parameters from the website www.dftb.org).

Dispersion interaction corrections can be introduced in the DFTB Hamiltonian using an empirical diatomic formulae. Two types of corrections are available in the deMonNano code and will be tested in the next section. The first one (hereafter labelled D1) is a

Lennard Jones type potential with short range corrections introduced by Zhechkov *et al.* [33]. The second one (hereafter labelled D2 [26]) is given by

$$E_{\text{disp}} = -\sum_{N}\sum_{\alpha,\beta} f_{\text{damp}}(|\mathbf{r}_\alpha - \mathbf{r}_\beta - \mathbf{R}_N|)\frac{C^6_{AB}}{|\mathbf{r}_\alpha - \mathbf{r}_\beta - \mathbf{R}_N|^6} \tag{19}$$

where $f_{\text{damp}}$ is a damping function screening the short range contribution and $C^6_{\alpha\beta}$ an empirical parameter (see [26] for details). In both cases, only the van der Waals contributions larger that $10^{-5}$ Hartree are taken into account, in order to limit the number N of boxes involved in the sum.

When calculations are performed with the WMull scheme, a value of $t_{CH} = 0.245$ has been determined to provide the atomic charges for the benzene molecule in agreement with reference calculations (see tables and discussion in reference [26]).

Regarding convergency criterions, we have used a tolerance of $10^{-8}$ for the atomic charges during the SCC process and $5.10^{-6}$ Hartree/Bohr for the largest gradient for local optimizations.

### *2.2. DFT calculations*

Dispersion corrected DFT calculations were performed under periodic boundary conditions using the Vienna *ab initio* simulation package (VASP [34–36]) together with PAW pseudopotentials [37,38] and the DFT-D3 semiempirical dispersion-corrected functional in its zero-damping formalism [39]. This functional has been chosen as it has been reported as a relevant choice for studies involving graphene [40]. A conjugate-gradient algorithm was used to relax the ions and the convergence criterion was set up so that the maximum atomic force was less than 0.01 eV $\text{Å}^{-1}$, all atoms being allowed to relax unconstrained. To avoid interactions between the benzene monomers/dimers and their periodic images, a cubic box measuring 50Å on a side was used for isolated systems. For supported ones, the calculations were performed on a 29.92Å x 34.55Å graphene surface (these values having been calculated on the basis of the graphene equilibrium lattice parameter reported in section 3.1) containing 392 carbon atoms placed in a 50 Å high simulation box to avoid any interaction between the adsorbed molecule and the underside of the graphene sheet of the upper periodic box. Since the size of the supercell was large enough, the Brillouin zone sampling in reciprocal space restricted to the Γ-point was sufficient to ensure good convergence of the total energy, except for the calculations aiming at determining the equilibrium parameters of the graphite bulk which required a 1x1x5 k-points grid. A plane-wave kinetic energy cut-off of 450 eV was employed. For dealing with the partial occupancies around the Fermi level, a Methfessel-Paxton smearing was used with $\sigma$ = 0.2 eV [41].

## 3. Results and discussion

In this section, we discuss the results of the DFTB calculations. All details about the dispersion-corrected DFT calculation performed to evaluate the quality of the DFTB calculations are given in the previous section, so that the computational details reported below only concern the DFTB calculations.

### *3.1. Graphene and Graphite*

In order to model graphene, we have first optimized the lattice parameter, working with a periodic box containing 392 atoms (∼30Å x 35Å x 50Å). For such a large simulation box, the Γ-point approximation remains valid as the energy varies by less than 3.4 $10^{-4}$ eV/atom (0.0008%) when going from one to three k-points in the x and y directions, and by less than 1.3 $10^{-4}$ eV/atom (0.0003%) when going from three to five k-points. The equilibrium C-C bond length determined with one or three k-points in x and y directions are the same at the precision of $10^{-3}$ Å . Values of 1.430±0.001 Å and 1.46±0.001 Å were

obtained with the DFTB-D1 and DFTB-D2 methods, respectively (see Table 1). These values are slighly larger than the value of 1.421 Å previously reported by Zhechkov *et al.* using the Γ-point approximation and a smaller unit cell [33]. The DFTB-D2 values gives the best agreement with the C-C bond length obtained at the DFT-D3 level (1.425±0.001 Å) as well as with the experimental values (1.42 Å).

The graphite bulk has been modeled by including two layers of the previously defined graphene sheet in the periodic box. In order to determine the appropriate number of k-points in the z direction (perpendicular to the graphene planes), we have performed single point energy calculations for an interlayer distance of 3.5 Å, chosen because it corresponds to the DFT-D3 one (3.488 Å, see Table 1), with one k-point in the x and y directions. The total energy varies by 2 $10^{-4}$ eV/atom (0.0004%) when the number of k-points is increased from one to three in the z direction, and then remains constant for calculations performed with five, seven and nine k-points in the z-direction. We have thus determined the equilibrium parameters of the graphite bulk with three k-points in the z directions (Table 1). Using either one or three k-points in the x and y directions led to the sames results at the target precision of 0.001 Å. The DFTB-D1 and DFTB-D2 C-C bond length are reduced by 0.001 Å with respect to their values in the graphene sheet, a trend also observed at the DFT-D3 level. The DFTB-D1 interlayer equilibrium distance (3.383±0.001 Å) is in agreement with both the value of reference [33] with a four layers model in the Γ-point approximation (3.38 Å) and the experimental data (3.356 Å). The interlayer distance is reduced to 3.131±0.001 Å at the DFTB-D2 level. With respect to theoretical references (DFT-D3, RPA and QMC) and experimental values, we can conclude that the DFTB-D1 method gives better quality results for the graphite interlayer distances, while the the DFTB-D2 method prevails for the C-C bond length.

**Table 1.** Graphene and Graphite structural data (in Å). *In these computational studies the $d_{C-C}$ distance was fixed to the one determined experimentally. ** Differences between the two DFTB-D1 calculations are detailed in the text.

| **Methods** | $\mathbf{d}_{C-C}^{Graphene}$ | $\mathbf{d}_{C-C}^{Graphite}$ | $\mathbf{d}_{interlayer}^{Graphite}$ |
|---|---|---|---|
| **DFTB-D1**** | 1.430±0.001 | 1.429±0.001 | 3.383±0.001 |
| **DFTB-D2** | 1.426±0.001 | 1.425±0.001 | 3.131±0.001 |
| **DFTB-D1**** | 1.421 [33] | 1.421 [33] | 3.38 [33] |
| **DFT-D3** | 1.425±0.001 | 1.424±0.001 | 3.488±0.001 |
| **RPA** | | 1.42* [42] | 3.34* [42] |
| **QMC** | | 1.42* [43] | 3.426* [43] |
| **Expt** | 1.42 [44] | 1.422 [45,46] | 3.356 [45,46] |

### *3.2. Benzene supported on Graphene*

We performed local structural optimisation for systems consisting of an isolated benzene molecule deposited on top of a graphene monolayer. On the basis of the results obtained in section 3.2, the calculations have been performed in the Γ-point approximation, the initial structures corresponding to a benzene molecule deposited in the proper orientation on the optimized graphene layer. Four different configurations have been probed, labelled $a_1, a_2, a_3, a_4$, which can be visualised in Figure 1. The three first ones correspond to the structures labelled $a_1, a_2, a_3$ in reference [47]; hollow, bridge, top in reference [48] and AA, SP and AB in reference [49]. The last structure $a_4$ was named top-rot in reference [48] and also studied in reference [50].

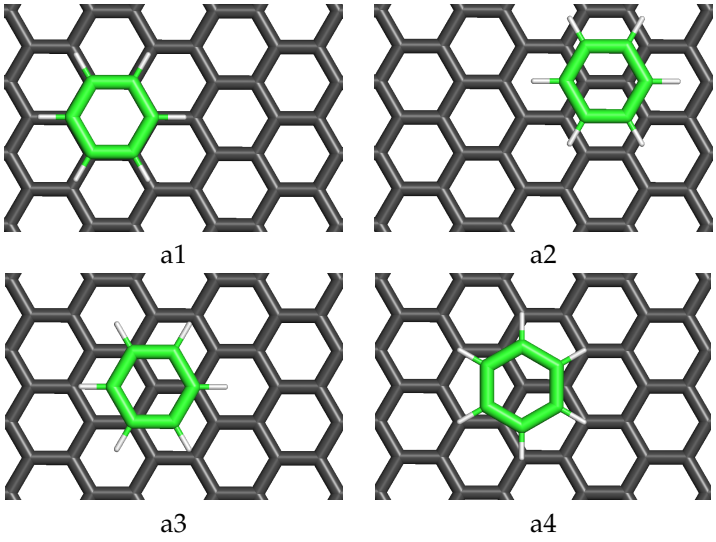


**Figure 1.** Isolated benzene molecule deposited on graphene.

**Table 2.** Binding energies of benzene on graphene in eV. The experimental binding energy of a benzene molecule on a graphite surface is -0.50±0.08 eV [51].

| **Method** | **a1** | **a2** | **a3** | **a4** |
|---|---|---|---|---|
| **DFTB-D1** | -0.639 | -0.652 | -0.654 | -0.651 |
| **DFTB-D2** | -0.439 | -0.448 | -0.447 | -0.451 |
| **DFT-D3** | -0.428 | -0.450 | -0.453 | -0.450 |
| **LDA** [47] | -0.16 | -0.23 | -0.24 | |
| $\omega$**B97X-D** [49] | | | -0.47 | |
| **optB86b-vdw** [50] | | | | -0.5 |
| **vdW-DF1** [48] | | | -0.49 | |
| **vdW-DF2** [48] | | | -0.43 | |
| **Expt. Saturated Adsorption Enthalpy** [50] | | | | -0.5 |

DFTB-D1 and DFTB-D2 results agree on the main trends, also present at the DFT-D3 level : three almost degenerated structures, namely $a_2, a_3$ and $a_4$, and the $a_1$ structure being less stable by about 0.012(DFTB-D2)/0.015(DFTB-D1)/0.025(DFT-D3) eV (see Table 2). The absolute binding energies provided by the DFTB-D2 scheme are in very good agreement with DFT results (appart from LDA) and experimental measurements. The DFTB-D1 scheme gives poorer results, with an overestimation of the binding energies of about 35% ($\sim$0.2 eV).

Regarding the z-separation between the benzene monomer and the graphene sheet (see table 3), DFTB-D1 and DFTB-D2 clearly underestimate the benzene-graphene distance by $\sim$0.35 Å. However, it should be noted that z-separations calculated with the dispersion corrected DFT functionals also significantly differ from each other by up to 0.25Å.

**Table 3.** Z-separation of Benzene on Graphene (in Å).

| **Method** | **a1** | **a2** | **a3** | **a4** |
|---|---|---|---|---|
| **DFTB-D1** | 3.152 | 3.133 | 3.130 | 3.138 |
| **DFTB-D2** | 3.080 | 3.073 | 3.081 | 3.054 |
| **DFT-D3** | 3.465 | 3.382 | 3.358 | 3.415 |
| $\omega$**B97X-D** [49] | 3.36 | 3.30 | 3.35 | |
| **vdW-DF1** [48] | | | 3.6 | |
| **vdW-DF2** [48] | | | 3.5 | |

### 3.3. Benzene dimers in vacuum

Reproducing the benzene dimer potential energy surface is a challenging task for DFT schemes, due to the fine competition between the various contributions to the total energy. This is even more true for approximated schemes like the DFTB method. Briefly, three characteristic structural families can be identified, namely sandwich (S), parallel-displaced (PD) and T-shaped (T), each one presenting several minima. In this work, the sandwich eclipsed (SE) structure has been selected to represent the sandwich family. The PD family is represented by the isomer shown in Figure 2 as it was previously reported to be the most stable of this family at the DFTB level. Two additional structures were considered to account for the T-shaped family, namely the T and Csoa isomers (corresponding to T4 and Csoa in reference [26]), which only differ by a slight displacement of the top benzene from a symetric position toward a position over a carbon atom. These two structures were previously reported to be degenerated as their energies differ by less than $10^{-3}$ eV at the DFTB level and the present DFT-D3 calculations show a difference of 8 $10^{-3}$ eV in favor of the Csoa isomer.

The binding energies for the different optimized structures are reported in Table 4 for both the DFTB, DFT-D3 and *ab initio* reference calculations (CCSD(T) and SAPT). In the case of the T-shaped family, only one of the two studied isomers could be located on the DFTB potential energy surfaces, namely Csoa with the DFTB-D1 method and T with the DFTB-D2 one. DFT-D3 and *ab initio* reference calculations agree on the fact that T-shaped and PD structures are close in energy and by far more stable than the SE structure. This ordering is not reproduced at the DFTB-D1 nor at the DFTB-D2 level, i.e. for the two dispersion corrections investigated in the absence of atomic charge corrections, because the SE structure is found to be almost degenerated with the PD structure and the T-shaped isomer is found to be the less stable one in both cases. Introducing the WMull charge correction detailed in section 1 with the D1 dispersion (DFTB-D1-WMull) makes the PD structure the most stable but the T-shaped structure remains the less stable. Finally, the DFTB-D2-WMull method provides a correct picture with the T-shaped and PD isomers being close in energy and more stable than the SE isomer. In addition, the binding energies are of the same order as those of the reference calculations.

**Table 4.** Binding energies for benzene dimer $bz_2$ in eV.

| **Method** | **T-shaped** | | **PD** | **SE** |
|---|---|---|---|---|
| **DFTB-D1** | Csoa | -0.126 | -0.194 | -0.192 |
| **DFTB-D1-WMull** | Csoa | -0.140 | -0.162 | -0.148 |
| **DFTB-D2** | T | -0.099 | -0.135 | -0.132 |
| **DFTB-D2-WMull** | T | -0.113 | -0.104 | -0.086 |
| **DFT-D3** | Csoa | -0.146 | -0.152 | -0.106 |
| | T | -0.138 | | |
| **CCSD(T)** [25] | Csoa | -0.12 | -0.12 | -0.07 |
| **SAPT** [25] | Csoa | -0.12 | -0.12 | -0.08 |

### 3.4. Benzene dimers supported on Graphene

It appeared from the previous sections that the DFTB-D2-WMull methods is the best choice for modelling at the DFTB level both an isolated benzene molecule deposited on a graphene layer and a benzene dimer in vacuum. This level of theory has thus been chosen to conduct the calculations aiming at investigating the deposition of a benzene dimer on a graphene sheet. Among the possible adsorption modes of a benzene molecule on a graphene monolayer, we selected the $a_4$ one as it was found to be the most stable at this level of theory (see section 3.2) and added a second benzene unit to form T, PD or SE configurations. The optimised structures, obtained in the Γ-point approximation, are shown in Figure 2.

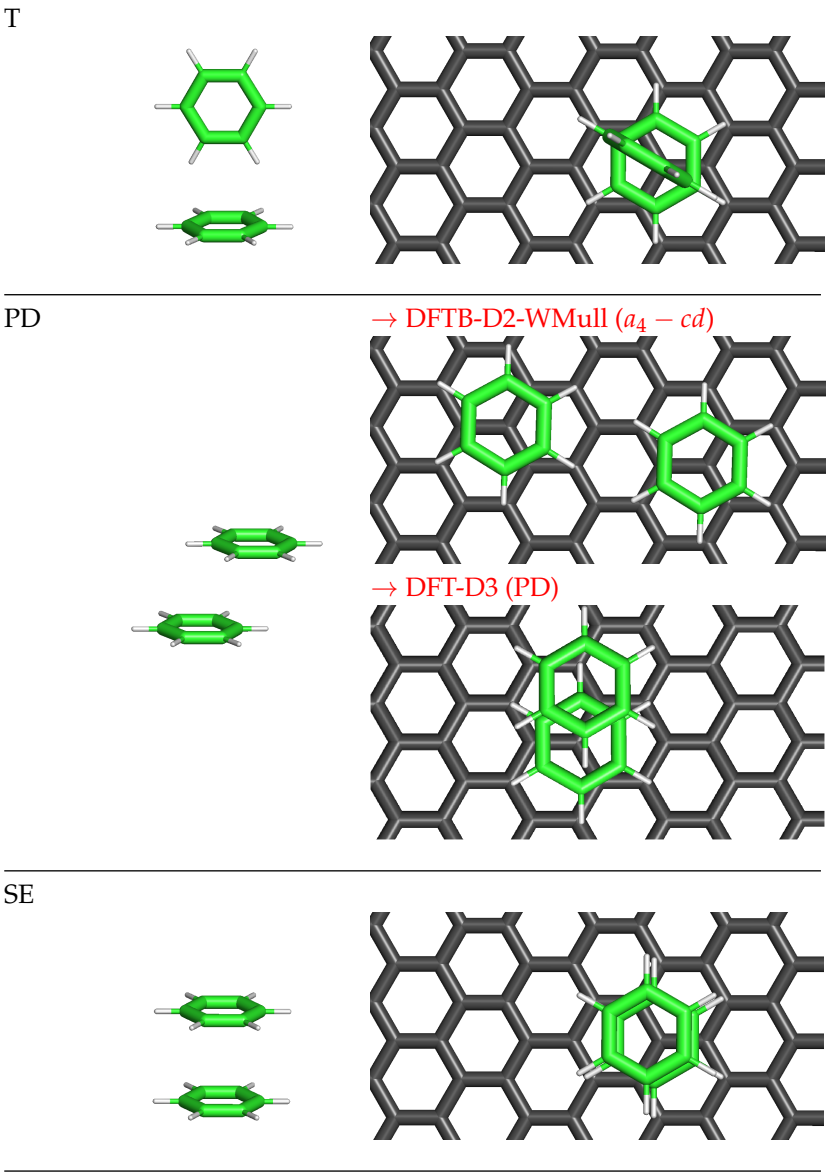


**Figure 2.** Benzene dimers $bz_2$ in vacuum and deposited on graphene

It can be seen that T and SE structures were preserved during the optimisation. On the opposite, the deposited PD dimer was stable at the DFT-D3 level only and led to a dissociated configuration at the DFTB-D2-WMull level in which the two benzene units are close to each other, both exhibiting a $a_4$ adsorption configuration on the graphene sheet. This configuration is hereafter named $a_4 - cd$ (close deposition on $a_4$ adsorption sites). In this latter, the hydrogen atom of each benzene molecule is pointing in-between two hydrogen atoms of the other benzene unit. Such a configuration limits the coulomb repulsion between the positively charged hydrogen atoms while preserving some attractive dispersion interactions.

**Table 5.** Binding energy of benzene dimers $bz_2$ on graphene in eV. * No value is reported at the DFTB-D2-WMull level for PD as the optimisation led to the $a_4 - cd$ structure.

| **Dissociation ref.** | **DFTB-D2-WMull** | | | | **DFT-D3** | | | |
|---|---|---|---|---|---|---|---|---|
| | **T** | **PD*** | $a_4 - cd$ | **SE** | **T** | **PD** | $a_4 - cd$ | **SE** |
| **graphene + 2bz** | -0.586 | ↳ | -0.929 | -0.573 | -0.605 | -0.624 | -0.938 | -0.583 |
| **graphene + $bz_2$** | -0.473 | ↳ | - | -0.487 | -0.467 | -0.473 | - | -0.478 |
| **graphene@bz + bz** | -0.135 | ↳ | -0.478 | -0.122 | -0.156 | -0.175 | -0.489 | -0.134 |
| **graphene@2bz** | 0.316 | ↳ | -0.027 | 0.329 | 0.294 | 0.275 | -0.039 | 0.316 |

The binding energies associated to the optimized structures are reported in Table 5 making use of various choices for the potential energy zeroth reference. In the first line (graphene + 2bz), the reference energy is the sum of the energies for an optimized graphene monolayer and two isolated benzene molecules. It appears that, at the DFT and DFTB levels, the most stable configuration relies on the dissociation of the benzene dimer to form the $a_4 - cd$ structure. The energetic difference between the T-shaped structure and the less stable SE dimer is twice smaller (0.013 eV vs 0.027 eV at the DFTB level and 0.022 eV vs 0.052 eV at the DFT level) when the dimer is deposited with respect to the gas phase condition. This is probably due to the interaction between the graphene surface and the benzene molecule that is furthest from the surface, which is favored in the sandwich configuration. In the second line (graphene + $bz_2$), the reference energy is that of an isolated graphene sheet plus that of the optimized dimer in its T, PD or SE form, respectively. The gained energy for the non-dissociating dimers (T and SE) are similar ($\sim$0.46-0.49 eV, for DFT and DFTB values), only very slighlty above the binding energy of a single benzene with graphene (0.45 eV for DFT and DFTB values). In the third line (graphene@bz + bz), the reference energy is that of a benzene deposited on a graphene sheet plus that of an isolated benzene. It differs from the isolated dimers by 0.022 eV for the T-shaped structure and 0.036 eV for the SE structure at the DFTB level and 0.018 eV and 0.028 eV at the DFT level. The larger value obtained for the SE dimer can be, again, related to the expected larger interaction energy between the graphene sheet and the second further benzene unit in the SE configuration. The last line (graphene@2bz) compares the binding energies with the one of a system where two benzene molecules would be deposited in $a_4$ configurations without interaction between them. This configuration appears to be more stable than those corresponding to the deposition of a T-shaped or SE dimer. The negative sign obtained for the $a_4 - cd$ structure shows that the latter is the most stable investigated configuration as it maximizes the interaction between each benzene molecule and the graphene surface while maintaining some stabilizing intermolecular interactions between the two benzene units. Again, this conclusion holds at both the DFT and DFTB levels. It should also be noted that the values of the interaction energies are of similar order for these two levels of calculation.

## 4. Conclusions

In the present paper, we have reported a new implementation of periodic boundary conditions in the DFTB code deMonNano, as only the Γ-point approximation was available in the previous version of the code. An originality of our scheme is the inclusion of atomic charge corrections which improves the description of intermolecular coulomb interactions. It allows to recover a reasonable description of molecular clusters, as shown in the particular case of benzene dimers in this work. Dispersion corrections are also mandatory for a proper description of such interactions and we have benchmarked two empirical correction schemes. One of them gives the best C-C bond distance in graphene and graphite whereas the second one provides the best interlayer distance in graphite, according to previous reference calculations and experiments, as well as with new DFT calculations performed with the DFT-D3 dispersion corrected functional.

Benzene monomer and dimers have been optimized at the DFTB and DFT levels, providing the following similar trends. For the deposition of a single benzene monomer

on a graphene sheet, the adsorption of the benzene centered on top of graphene carbon atom or C-C bond leads to almost degenerated structures, by far more stable than the superimposition of the benzene on top of a graphene aromatic cycle. The most stable one at the DFTB level has been selected to build initial conditions for benzene dimers deposition on graphene. The structural energy gap between the most stable T-shaped dimer and less stable Sandwich-like dimer is divided by two when the cluster is supported on graphene. The supported Parallel-Displaced structure appeared to be not stable at the DFTB level, leading to a structure where the two benzene are deposited close to each other on the graphene surface. This structure is the most stable one of our calculations at DFT and DFTB levels, also more stable than the deposition of two benzene monomer at infinite distance, which is not the case of the deposited sandwich or T-shaped dimers. As a conclusion, we have shown the ability of the new implementation to characterize properties of molecular clusters deposited on surfaces.

**Acknowledgments:** This work was granted access to the HPC resources of CALMIP supercomputing center under the allocations p18009.

**Conflicts of Interest:** The authors declare no conflict of interest.

## References

1. Sadowska, M.; Cieśla, M.; Adamczyk, Z. Nanoparticle deposition on heterogeneous surfaces: Random sequential adsorption modeling and experiments. *Colloids and Surfaces A: Physicochemical and Engineering Aspects* **2021**, *617*, 126296. doi:10.1016/j.colsurfa.2021.126296.
2. Li, L.; Plessow, P.N.; Rieger, M.; Sauer, S.; Sánchez-Carrera, R.S.; Schaefer, A.; Abild-Pedersen, F. Modeling the Migration of Platinum Nanoparticles on Surfaces Using a Kinetic Monte Carlo Approach. *The Journal of Physical Chemistry C* **2017**, *121*, 4261–4269. doi:10.1021/acs.jpcc.6b11549.
3. Rochefort, A.; Vernisse, L.; Gómez-Herrero, A.C.; Sánchez-Sánchez, C.; Martín-Gago, J.A.; Chérioux, F.; Clair, S.; Coraux, J.; Martínez, J.I. Role of the Structure and Reactivity of Cu and Ag Surfaces in the Formation of a 2D Metal–Hexahydroxytriphenylene Network. *The Journal of Physical Chemistry C* **2021**, *125*, 17333–17341. doi:10.1021/acs.jpcc.1c03976.
4. Bruix, A.; Margraf, J.; Andersen, M.; K., R. First-principles-based multiscale modelling of heterogeneous catalysis. *Nature Catalysis* **2019**, *2*, 659–670. doi:10.1038/s41929-019-0298-3.
5. Abidi, N.; Lim, K.R.G.; Seh, Z.W.; Steinmann, S.N. Atomistic modeling of electrocatalysis: Are we there yet? *WIREs Computational Molecular Science* **2021**, *11*, e1499. doi:10.1002/wcms.1499.
6. Zhang, C.; Chen, G.; Si, Y.; Liu, M. Surface modeling of photocatalytic materials for water splitting. *Physical Chemistry Chemical Physics* **2022**, *24*, 1237–1261. doi:10.1039/D1CP04352H.
7. Vilan, A.; Cahen, D. Chemical Modification of Semiconductor Surfaces for Molecular Electronics. *Chemical Reviews* **2017**, *117*, 4624–4666. PMID: 28230354, doi:10.1021/acs.chemrev.6b00746.
8. Shahmoradi, A.; Ahangari, M.G.; Jahanshahi, M.; Mirghoreishi, M.; Fathi, E.; Mashhadzadeh, A.H. Removal of methylmercaptan pollution using Ni and Pt-decorated graphene: an ab-initio DFT study. *Journal of Sulfur Chemistry* **2020**, *41*, 593–604. doi:10.1080/17415993.2020.1780236.
9. Li, M.; Zhu, H.; Wei, G.; He, A.; Liu, Y. DFT calculation and analysis of the gas sensing mechanism of methoxy propanol on Ag decorated SnO2 (110) surface. *RSC Advances* **2019**, *9*, 35862–35871. doi:10.1039/C9RA02958C.
10. Soini, T.M.; Rösch, N. Size-dependent properties of transition metal clusters: from molecules to crystals and surfaces – computational studies with the program ParaGauss. *Physical Chemistry Chemical Physics* **2015**, *17*, 28463–28483. doi:10.1039/C5CP04281J.
11. Porezag, D.; Frauenheim, T.; Köhler, T.; Seifert, G.; Kaschner, R. Construction of tight-binding-like potentials on the basis of density-functional theory: Application to carbon. *Physical Review B* **1995**, *51*, 12947–12957. doi:10.1103/PhysRevB.51.12947.
12. Seifert, G.; Porezag, D.; Frauenheim, T. Calculations of molecules, clusters, and solids with a simplified LCAO-DFT-LDA scheme. *International Journal of Quantum Chemistry* **1996**, *58*, 185–192. doi:10.1002/(SICI)1097-461X(1996)58:2<185::AID-QUA7>3.0.CO;2-U.

13. Elstner, M.; Seifert, G. Density functional tight binding. *Philosophical Transactions of the Royal Society A: Mathematical, Physical and Engineering Sciences* **2014**, *372*, 20120483. doi: 10.1098/rsta.2012.0483.
14. Spiegelman, F.; Tarrat, N.; Cuny, J.; Dontot, L.; Posenitskiy, E.; Martí, C.; Simon, A.; Rapacioli, M. Density-functional tight-binding: basic concepts and applications to molecules and clusters. *Advances in Physics: X* **2020**, *5*, 1710252. doi:10.1080/23746149.2019.1710252.
15. Aradi, B.; Hourahine, B.; Frauenheim, T. DFTB+, a Sparse Matrix-Based Implementation of the DFTB Method. *Journal of Physical Chemistry A* **2007**, *111*, 5678–5684. PMID: 17567110, doi: 10.1021/jp070186p.
16. Koskinen, P.; Makinen, V. Density-Functional Tight-Binding for Beginners. *Computational Materials Science* **2009**, *47*, 237–253. doi:10.1016/j.commatsci.2009.07.013.
17. te Velde, G.; Bickelhaupt, F.M.; Baerends, E.J.; Fonseca Guerra, C.; van Gisbergen, S.J.A.; Snijders, J.G.; Ziegler, T. Chemistry with ADF. *Journal of Computational Chemistry* **2001**, *22*, 931–967. doi:10.1002/jcc.1056.
18. Salomon-Ferrer, R.; Case, D.A.; Walker, R.C. An overview of the Amber biomolecular simulation package. *WIREs Computational Molecular Science* **2013**, *3*, 198–210. doi: 10.1002/wcms.1121.
19. Walker, R.C.; Crowley, M.F.; Case, D.A. The implementation of a fast and accurate QM/MM potential method in Amber. *Journal of Computational Chemistry* **2008**, *29*, 1019–1031. doi: 10.1002/jcc.20857.
20. Berendsen, H.; van der Spoel, D.; van Drunen, R. GROMACS: A message-passing parallel molecular dynamics implementation. *Computer Physics Communications* **1995**, *91*, 43 – 56. doi: 10.1016/0010-4655(95)00042-E.
21. Hutter, J.; Iannuzzi, M.; Schiffmann, F.; VandeVondele, J. cp2k: atomistic simulations of condensed matter systems. *WIREs Computational Molecular Science* **2014**, *4*, 15–25. doi: 10.1002/wcms.1159.
22. Heine, T.; Rapacioli, M.; Patchkovskii, S.; Frenzel, J.; Koster, A.; Calaminici, P.; Duarte, H.A.; Escalante, S.; Flores-Moreno, R.; Goursot, A.; Reveles, J.; Salahub, D.; Vela, A. *deMonNano, http:demon-nano.ups-tlse.fr* **2009**.
23. Peeters, E.; Hony, S.; Van Kerckhoven, C.; Tielens, A.G.G.M.; Allamandola, L.J.; Hudgins, D.M.; Bauschlicher, C.W. The rich 6 to 9 $\mu$m spectrum of interstellar PAHs. *Astronomy & Astrophysics* **2002**, *390*, 1089–1113. doi:10.1051/0004-6361:20020773.
24. Rapacioli, M.; Joblin, C.; Boissel, P. Spectroscopy of polycyclic aromatic hydrocarbons and very small grains in photodissociation regions*. *Astronomy & Astrophysics* **2005**, *429*, 193–204. doi:10.1051/0004-6361:20041247.
25. Podeszwa, R.; Bukowski, R.; Szalewicz, K. Potential Energy Surface for the Benzene Dimer and Perturbational Analysis of pi-pi Interactions. *The Journal of Physical Chemistry A* **2006**, *110*, 10345–10354. doi:10.1021/jp064095o.
26. Rapacioli, M.; Spiegelman, F.; Talbi, D.; Mineva, T.; Goursot, A.; Heine, T.; Seifert, G. Correction for dispersion and Coulombic interactions in molecular clusters with density functional derived methods: Application to polycyclic aromatic hydrocarbon clusters. *The Journal of Chemical Physics* **2009**, *130*, 244304. doi:10.1063/1.3152882.
27. Elstner, M.; Porezag, D.; Seifert, G.; Frauenheim, T.; Suhai, S. Self Consistent-Charge Density-Functional Tight-Binding Method for Simulations of Biological Molecules. *MRS Proceedings* **1998**, *538*, 541. doi:10.1557/PROC-538-541.
28. Yang, Y.; Yu, H.; York, D.; Cui, Q.; Elstner, M. Extension of the self-consistent-charge density-functional tight-binding method: third-order expansion of the density functional theory total energy and introduction of a modified effective coulomb interaction. *Journal of Physical Chemistry A* **2007**, *111*, 10861–10873. doi:10.1021/jp074167r.
29. Li, J.; Zhu, T.; Cramer, C.; Truhlar, D. New Class IV Charge Model for Extracting Accurate Partial Charges from Wave Functions. *Journal of Physical Chemistry A* **1998**, *102*, 1820–1831. doi:10.1021/jp972682r.
30. Michoulier, E.; Ben Amor, N.; Rapacioli, M.; Noble, J.A.; Mascetti, J.; Toubin, C.; Simon, A. Theoretical determination of adsorption and ionisation energies of polycyclic aromatic hydrocarbons on water ice. *Physical Chemistry Chemical Physics* **2018**, *20*, 11941–11953. doi: 10.1039/C8CP01175C.
31. Dontot, L.; Spiegelman, F.; Zamith, S.; Rapacioli, M. Dependence upon charge of the vibrational spectra of small Polycyclic Aromatic Hydrocarbon clusters: the example of pyrene. *The European Physical Journal D* **2020**, *74*, 216. doi:10.1140/epjd/e2020-10081-0.

32. Simon, A.; Rapacioli, M.; Michoulier, E.; Zheng, L.; Korchagina, K.; Cuny, J. Contribution of the density-functional-based tight-binding scheme to the description of water clusters: methods, applications and extension to bulk systems. *Molecular Simulation* **2019**, *45*, 249–268. doi:10.1080/08927022.2018.1554903.
33. Zhechkov, L.; Heine, T.; Patchkovskii, S.; Seifert, G.; Duarte, H.A. An Efficient a Posteriori Treatment for Dispersion Interaction in Density-Functional-Based Tight Binding. *Journal of Chemical Theory and Computation* **2005**, *1*, 841–847. doi:10.1021/ct050065y.
34. Kresse, G.; Hafner, J. *Ab initio* molecular dynamics for liquid metals. *Physical Review B* **1993**, *47*, 558–561. doi:10.1103/PhysRevB.47.558.
35. Kresse, G.; Furthmüller, J. Efficiency of ab-initio total energy calculations for metals and semiconductors using a plane-wave basis set. *Computational Materials Science* **1996**, *6*, 15–50. doi:10.1016/0927-0256(96)00008-0.
36. Kresse, G.; Furthmüller, J. Efficient iterative schemes for *ab initio* total-energy calculations using a plane-wave basis set. *Physical Review B* **1996**, *54*, 11169–11186. doi:10.1103/PhysRevB.54.11169.
37. Blöchl, P.E. Projector augmented-wave method. *Physical Review B* **1994**, *50*, 17953–17979. doi:10.1103/PhysRevB.50.17953.
38. Kresse, G.; Joubert, D. From ultrasoft pseudopotentials to the projector augmented-wave method. *Physical Review B* **1999**, *59*, 1758–1775. doi:10.1103/PhysRevB.59.1758.
39. Grimme, S.; Antony, J.; Ehrlich, S.; Krieg, H. A consistent and accurate ab initio parametrization of density functional dispersion correction (DFT-D) for the 94 elements H-Pu. *The Journal of Chemical Physics* **2010**, *132*, 154104. doi:10.1063/1.3382344.
40. Lebedeva, I.V.; Lebedev, A.V.; Popov, A.M.; Knizhnik, A.A. Comparison of performance of van der Waals-corrected exchange-correlation functionals for interlayer interaction in graphene and hexagonal boron nitride. *Computational Materials Science* **2017**, *128*, 45–58. doi:10.1016/j.commatsci.2016.11.011.
41. Methfessel, M.; Paxton, A.T. High-precision sampling for Brillouin-zone integration in metals. *Physical Review B* **1989**, *40*, 3616–3621. doi:10.1103/PhysRevB.40.3616.
42. Lebègue, S.; Harl, J.; Gould, T.; Ángyán, J.G.; Kresse, G.; Dobson, J.F. Cohesive Properties and Asymptotics of the Dispersion Interaction in Graphite by the Random Phase Approximation. *Physical Review Letters* **2010**, *105*, 196401. doi:10.1103/PhysRevLett.105.196401.
43. Spanu, L.; Sorella, S.; Galli, G. Nature and Strength of Interlayer Binding in Graphite. *Physical Review Letters* **2009**, *103*, 196401. doi:10.1103/PhysRevLett.103.196401.
44. Cooper, D.R.; D'Anjou, B.; Ghattamaneni, N.; Harack, B.; Hilke, M.; Horth, A.; Majlis, N.; Massicotte, M.; Vandsburger, L.; Whiteway, E.; Yu, V. Experimental Review of Graphene. *ISRN Condensed Matter Physics* **2012**, *2012*, 501686. doi:10.5402/2012/501686.
45. Bosak, A.; Krisch, M.; Mohr, M.; Maultzsch, J.; Thomsen, C. Elasticity of single-crystalline graphite: Inelastic x-ray scattering study. *Physical Review B* **2007**, *75*, 153408. doi:10.1103/PhysRevB.75.153408.
46. Trucano, P.; Chen, R. Structure of graphite by neutron diffraction. *Nature* **1975**, *258*, 136–137. doi:10.1038/258136a0.
47. Zhang, Y.H.; Zhou, K.G.; Xie, K.F.; Zeng, J.; Zhang, H.L.; Peng, Y. Tuning the electronic structure and transport properties of graphene by noncovalent functionalization: effects of organic donor, acceptor and metal atoms. *Nanotechnology* **2010**, *21*, 065201. doi:10.1088/0957-4484/21/6/065201.
48. Berland, K.; Hyldgaard, P. Analysis of van der Waals density functional components: Binding and corrugation of benzene and $C_{60}$ on boron nitride and graphene. *Physical Review B* **2013**, *87*, 205421. doi:10.1103/PhysRevB.87.205421.
49. Ershova, O.V.; Lillestolen, T.C.; Bichoutskaia, E. Study of polycyclic aromatic hydrocarbons adsorbed on graphene using density functional theory with empirical dispersion correction. *Physical Chemistry Chemical Physics* **2010**, *12*, 6483–6491. doi:10.1039/C000370K.
50. Otyepková, E.; Lazar, P.; Čépe, K.; Tomanec, O.; Otyepka, M. Organic adsorbates have higher affinities to fluorographene than to graphene. *Applied Materials Today* **2016**, *5*, 142–149. doi:10.1016/j.apmt.2016.09.016.
51. Zacharia, R.; Ulbricht, H.; Hertel, T. Interlayer cohesive energy of graphite from thermal desorption of polyaromatic hydrocarbons. *Physical Review B* **2004**, *69*, 155406. doi:10.1103/PhysRevB.69.155406.